Computational Fluid Dynamics Study of a Complete Coal Direct Chemical Looping Sub-Pilot Unit

Wadhwani, Rahul*⁺; Mohanty, Bikash

Department of Chemical Engineering, Indian Institute of Technology, Roorkee-247667, INDIA

ABSTRACT: *The present Computational Fluid Dynamics (CFD) work deals with the modeling of complete coal direct chemical looping sub-pilot unit which use coal as fuel and ferric oxide supported on alumina as an oxygen carrier. The 2D CFD model of the complete arrangement incorporating both fuel and air reactors and their inter-connecting parts was solved using FLUENT. The CFD model was run with two different sets of reactions - the first set with eleven and second set with eighteen reactions. Computed results for second set of reactions were found to be in good agreement with the published pilot plant data. The CFD model with second set of reactions predicted fuel conversion for Sub-Bituminous Coal (SBC) and Metallurgical Coke (MC) were 95.39% and 87.07% respectively while, the published results were 97-99% and 70-99% respectively. Further, the purity of CO_2 in fuel reactor exhaust were 92.34% and 90.19%, while, the published were 99.8% and 99.6% for SBC & MC respectively.*

KEYWORDS: *Coal direct chemical looping; Oxygen carrier; CFD; Metallurgical Coke (MC); Sub-Bituminous Coal (SBC).*

INTRODUCTION

The exponential rising trend in energy consumption compounded with deteriorating quality of fossil fuel have forced scientists to seeks for alternate solutions to deal with the problems related to energy crises and greenhouse gases emission. Additionally, the clean and renewable sources of energy like the solar, the wind, and the geothermal energy are unlikely to meet the currently mounting energy demand in foreseeable future due to the constraints associated with such renewable energy. Furthermore, the constraint on nuclear power of its spent fuel management and susceptibility to catastrophic hazards makes it implausible to play a vital role

in meeting future energy demand. Hence, fossil fuels hold as the key source of energy in near future. [1]

The carbon emission from fossil fuel estimated by IPCC [2] has posed considerable challenge for researchers and scientists in the past decade. The applications of clean technologies such as chemical looping combustion, fuel cells and similar technologies are becoming an attractive proposition in foreseeable future. The abundance of coal (for ~150 years) and its regionally controlled cheap cost, offers an attractive proposition for clean coal based technologies like coal direct chemical looping combustion.

Traditional technologies to generate electricity from coal generates flue gases consist lean amount of carbon dioxide whose separation is expensive and technically cumbersome. While, in the chemical looping technology, carbon dioxide is available as a directly sequestration ready stream, and hence supports the cost effectiveness. Since late 1990s the chemical looping process has gained momentum and has been targeted mainly towards efficient carbon capturing, hydrogen, and power generation [3].

In 2006, *Abad et al.* [4] published the result of a continuously operating 300W chemical looping combustion unit based on natural gas/syngas as fuel and Mn_3O_4 supported on $Mg-ZrO_2$ as an oxygen carrier. *Berguerand et al.* [5] in 2008 carried out their study on a 10 kW_{th} chemical looping combustion unit using petroleum-coke as solid fuel and ilmenite as an oxygen carrier and observed that CO_2 capture capacity is in the range of 60-75% and 66-78% solid fuel conversion. *Kim et al.* [6] reported the design criteria and operating conditions of a 25 kW_{th} sub-pilot plant using two fuels SBC and MC with ferric oxide supported on alumina as an oxygen carrier was used. They observed both US based coal provide more than 90% maximum fuel conversion and ~99% pure CO_2 in exhaust.

Deng et al. [7] carried out CFD based simulation study on reaction kinetics of chemical looping combustion using FLUENT for fuel reactor only and demonstrated the effect of particle diameter, gas flow rate, and bed temperature on fuel conversion. *Kruggel-Emden et al.* [8] conducted an interconnected multiphase CFD simulation study of chemical looping combustion using methane as fuel and Mn_3O_4 supported on $Mg-ZrO_2$ as an oxygen carrier using bubbling fluidized bed and riser as fuel and air reactor separately. They considered the time-dependent mass exchanges between the two reactors through inlet and outlet boundary conditions in place continuous exchange.

Considerable work has been carried out in this field [9-14], there appears to be a gap study of the complete looping process through CFD so that the interaction between the various sections is visible. CFD simulations were carried out in two sets of reactions to bridge the above gap, in the first set the simulation was done taking eleven reactions into account as proposed by *Kim et al.* [6] and the resulting simulated results were validated with the sub-pilot plant results.
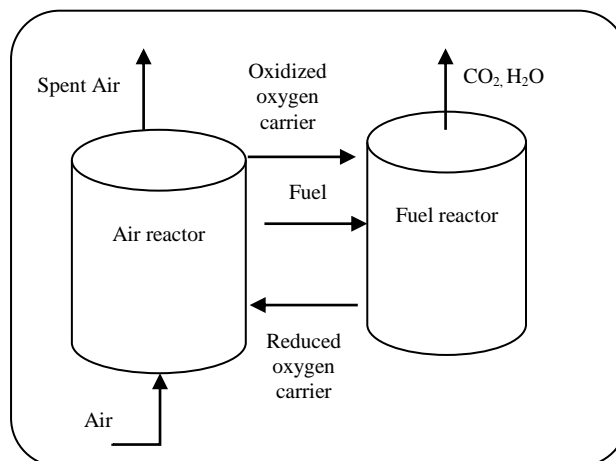

Fig. 1: Coal direct chemical looping process.

A search in this regard by *Wadhwani* [15] shows that a few significant reactions of by-products are required to model the system accurately. In the second set, seven significant reactions proposed were included to the first set of eleven reactions. The simulated results thus obtained were validated against the sub-pilot plant results. The outcome achieved with the second set were in better agreement with the sub-pilot plant data as compared to the first set.

PROCESS DESCRIPTION

In the chemical looping combustion process, carbonaceous fuel such as coal; first reacts with a metal oxide which acts as an oxygen carrier in the fuel reactor section which is thus subsequently get reduced to metal or lower oxidation state. Hence, producing carbon dioxide and steam as major products, as carbon dioxide is readily separable from the mixture by condensing steam. The reduced metal from the fuel reactor is thus oxidized again by air/oxygen in the air reactor section and regenerate to metal oxide(s) which are then recycled back to the fuel reactor section for reuse. The cyclic process used to describe the above process showed in Fig. 1.

PROBLEM DESCRIPTION

The geometrical as well as operating parameters of a 25 kW_{th} sub-pilot plant developed at Ohio State University, USA [6] were considered for the present CFD simulation. The details of dimensions used computed from the equivalent volume of each section described by *Kim et al.* [6]. The geometry used in our study shown

Table 1: Geometry Parameters.

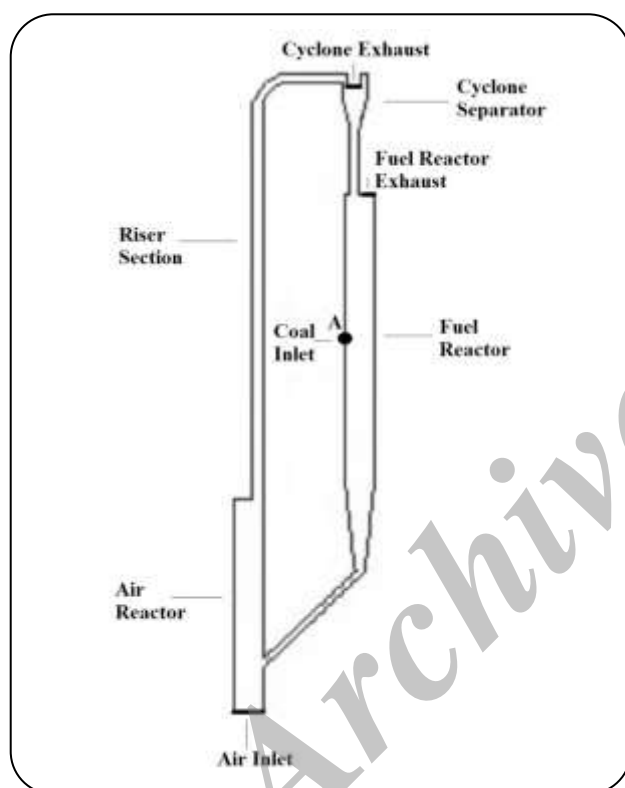|	
Fuel Reactor Height	3.37m
Fuel Reactor Diameter	0.34m
Air Reactor Height	1.88m
Air Reactor Diameter	0.33m
Tube Diameter	0.11m
Riser Height	4.68m
Cyclone Separator Total Height	0.62m
Cyclone Separator Diameter	0.28m

Fig. 2: Sub-pilot unit of present problem.

in Fig. 2 with their dimension detailed in Table 1. Two fuels namely SBC and MC were used one at a time in the pilot plant with ferric oxide as an oxygen carrier.

Table 2 and Table 3 described the proximate analysis and ultimate analysis (on dry basis) for two types of coal i.e. MC and SBC respectively, which used in this study [6]. Table 4 provides the details about the properties of oxygen carrier that was utilized in the pilot plant and also taken into account or the present study.

MODEL DEVELOPMENT

A 2-D CFD model for interconnected fuel and air reactor was developed on commercial computational software FLUENT 6.3.26 and mesh for above assembly was created using GAMBIT 2.3.16. The solid-gas mixture containing solid particles (fuel and oxygen carrier) in the range of 36-1500μm along with the volume gases injected into the system as well as created from the reaction which amounts nearly 94% by volume of the solid-gas mixture. These were assumed to flow as a fluid inside both the reactors and their interconnecting parts while the kinetic parameters of solid-solid reactions were incorporated to minimize the effect of assumption. Eleven reactions, as given in Table 5 and reported by *Kim et al.* [6], were considered as the first set. Supplement to the above reactions, seven other reactions proposed by *Wadhwani* [15] include in the second set (Given in Table 6).

Before a complicated two phase and 3D CFD model carefully chosen for the accurate analysis of the present problem, it was thought logical to use the least complicated 2D CFD model. This step is reasonable due to least amount of published information for simulation and the major volume of gaseous species (~94% by volume). The solid-gas mixture flow mostly as a gas mixture while incorporation of kinetic parameters for reaction between solid-solid incorporated to lower the impact of assumption. Hence, the Species-Transport model with volumetric reactions used to find out the extent of agreement it offers to the pilot plant data. Following governing equations were solved on commercial available software FLUENT 6.3.26 for the present model:

Mass Conservation Equation:

The equation for mass conservation/continuity equation can be written as:

$$\frac{\partial p}{\partial t} + \nabla \cdot \left(\rho \vec{v} \right) = S_m \tag{1}$$

The mass conservation Eq. (1) is valid for compressible and incompressible flows.

Momentum Conservation Equations:

In an inertial frame, the momentum conservation equation is described as below Eq. 2:

141

Table 2: Proximate Analysis of fuels.

	Proximate Analysis (Dry Basis)	
	MC	SBC
Ash	16.99%	11.38%
Volatile Matter	8.55%	39.57%
Fixed Carbon	74.47%	49.05%
Energy Value	28,108 kJ/kg	26,047 kJ/kg
Energy Value[1]	33,857 kJ/kg	29,391 kJ/kg
Average Particle Size	36.5 μm	89.8 μm
Moisture	2.69%	10.53%

Table 3: Ultimate Analysis of fuels.

	Ultimate Analysis (Dry Basis)	
	MC	SBC
Carbon	75.89%	65.5%
Hydrogen	1.62%	4.41%
Nitrogen	0.78%	0.78%
Sulfur	0.5%	0.77%
Oxygen	4.22%	17.16%

Table 4: Properties of oxygen carrie.

Reactive oxygen carrier	Fe_2O_3
Weight content of reactive oxygen carrier	40-60%
Particle size of oxygen carrier	1.5 mm
Supporting oxygen carrier	Al_2O_3
Density of oxygen carrier	4724 kg/m³

$$\frac{\partial(\rho\vec{v})}{\partial t} + \nabla\cdot(\rho\vec{v}\vec{v}) = -\nabla\cdot\left(\overline{\overline{\tau}}\right) + p\vec{g} + \vec{F} \tag{2}$$

The stress tensor $\overline{\overline{\tau}}$ is given by Eq. 3

$$\overline{\overline{\tau}} = \mu\left[\left(\nabla\vec{v} + \nabla\vec{v}^T\right) - \frac{2}{3}\nabla.\vec{v}I\right] \tag{3}$$

The second term on the right hand side of Eq. 3 is the effect of volume dilation.

Energy Conservation Equation:

The conservation of Energy is defined by the following Eq. 4:

$$\frac{\partial(\rho E)}{\partial t} + \nabla\cdot\left(\vec{v}(\rho E + p)\right) = \tag{4}$$

$$\nabla\cdot\left(k_{eff}\nabla T - \sum_j h_j\vec{J}_j + \left(\overline{\overline{\tau}}_{eff}\cdot\vec{v}\right)\right) + S_h$$

In Eq. 4,

$$E = h - \frac{p}{\rho} + \frac{v^2}{2} \tag{5}$$

The sensible enthalpy is defined as:
For ideal gases as:

$$h = \sum_j Y_j h_j \tag{6}$$

142

Table 5: Reactions proposed by [9] for coal direct chemical looping process.

Reaction No.	Reaction	E_R (J/kmol)
1.	$Coal \rightarrow C + CH_4 + NO_2 + SO_2 + CO_2 + H_2O$	
1.1	For MC: $C_{7.61}H_{1.935}N_{0.067}S_{0.019}O_{0.318} \rightarrow 7.11325C + 0.45375CH_4 + 0.067NO_2 + 0.019SO_2 + 0.043CO_2 + 0.06H_2O$	7.74×10^7
1.2	For SBC: $C_{6.154}H_{4.391}N_{0.063}S_{0.027}O_{1.211} \rightarrow 4.59675C + 1.13275CH_4 + 0.063NO_2 + 0.027SO_2 + 0.42CO_2 + 0.191H_2O$	1.14×10^8
2.	$2Fe_2O_3 + C \rightarrow 4FeO + CO_2$	3.0124×10^8
3.	$4Fe_2O_3 + CH_4 \rightarrow 4FeO + 2H_2O + CO_2$	1.352×10^8
4.	$Fe_2O_3 + CO \rightarrow 2FeO + CO_2$	8.07×10^7
5.	$Fe_2O_3 + H_2 \rightarrow 2FeO + H_2O$	6.5×10^7
6.	$FeO + CO \rightarrow Fe + CO_2$	1.205×10^7
7.	$FeO + H_2 \rightarrow Fe + H_2O$	2.151×10^7
8.	$C + CO_2 \rightarrow 2CO$	2.11×10^8
9.	$C + H_2O \rightarrow CO + H_2$	2.31×10^8
10.	$2Fe + 1.5O_2 \rightarrow Fe_2O_3$	2.025×10^7
11.	$2FeO + 0.5O_2 \rightarrow Fe_2O_3$	2.55×10^7

Table 6: Other significant reactions for coal direct chemical looping process.

Reaction No.	Reaction	E_R (J/kmol)
12.	$C + 2H_2 \rightarrow CH_4$	1.5×10^8
13.	$CO + H_2O \rightleftharpoons CO_2 + H_2$	1.26×10^7
14.	$CH_4 + H_2O \rightleftharpoons CO + 3H_2$	3×10^7
15.	$C + O_2 \rightarrow CO_2$	1.794×10^8
16.	$CO + 0.5O_2 \rightarrow CO_2$	1.674×10^8
17.	$2FeO + H_2O \rightarrow Fe_2O_3 + H_2$	7.79×10^7
18.	$2H_2 + O_2 \rightarrow 2H_2O$	2.852×10^7

In Eq. 6, h_j at $T_{ref} = 298.15K$ is defined as:

$$h_j = \int_{T_{ref}}^{T} c_{p,j} dT \tag{7}$$

Species Transport Equations:

The local mass fraction of each species (Y_i) through the solution of a convection-diffusion equation for the i th species is solved. It takes the following general form:

$$\frac{\partial}{\partial t}(\rho Y_i) + \nabla \cdot (\rho \vec{v} Y_i) = \nabla \cdot \vec{J}_t + R_i + S_i \tag{8}$$

Mass Diffusion in Laminar Flows:

In the above Eq. (8), which arises due to concentration gradients; in the present model, dilute approximation was assumed, which is defined as follows:

$$\vec{J}_t = -\rho D_{i,m} \nabla Y_i \tag{9}$$

The Laminar Finite-Rate Model:

The net source of chemical species i th due to reaction is computed as the sum of the Arrhenius reaction sources over the N_R reactions that the species participate in:

$$R_i = M_{w,i} \sum_{r=1}^{N_R} R_{t,r} \tag{10}$$

For a non-reversible reaction, the molar rate of creation/destruction of specie i in reaction r ($\widehat{R_{i,r}}$ in Eq. (10)) is given by

$$\widehat{R_{i,r}} = \Gamma\left(v_{i,r}^{''} - v_{i,r}'\right)\left(k_{f,r}\,\Pi_{j=1}^{N}[C_{j,r}]^{\left(\eta_{j,r}' + \eta_{j,r}^{''}\right)}\right) \tag{11}$$

For a reversible reaction, the molar rate of creation/destruction of species i in reaction r, is given by

$$\widehat{R_{i,r}} = \Gamma\left(v_{i,r}^{''} - v_{i,r}'\right)\left(k_{f,r}\,\Pi_{j=1}^{N}[C_{j,r}]^{\eta_{j,r}'}\right. \tag{12}$$

$$\left. - k_{b,r}\Pi_{j=1}^{N}\left[C_{j,r}\right]^{\left(v_{j,r}^{''}\right)}\right)$$

The rate exponent for the reverse reaction part in Eq. (12) is always the product species stoichiometric coefficient ($v''_{j,r}$).

$$k_{f,r}\sum_{j=1}^{N}\gamma_{j,r}C_{j} \tag{13}$$

The forward rate constant $k_{f,r}$ for reaction r, is computed using the Arrhenius expression

$$k_{f,r} = A_{r}T^{\beta_{r}}e^{-ER/RT} \tag{14}$$

For reversible reactions, the backward rate constant $k_{b,r}$ for reaction *r*, is computed from the forward rate constant using the following relation:

$$k_{b,r} = \frac{k_{f,r}}{K_{r}} \tag{15}$$

The value of K_r is computed from the following Eq. (16):

$$K_{r} = e^{\left(\frac{\Delta S_{r}^{o}}{R} - \frac{\Delta H_{r}^{o}}{RT}\right)}\left(\frac{P_{atm}}{RT}\right)^{\sum_{i,r}^{N}\left(v_{i,r}^{''} - v_{i,r}'\right)} \tag{16}$$

Where, the term within the exponential function represents the change in Gibbs free energy, and its components are computed as follows:

$$\frac{\Delta S_{r}^{o}}{R} = \sum_{i=1}^{N}\left(v_{i,r}^{''} - v_{i,r}'\right)\frac{S_{i}^{o}}{R} \tag{17}$$

$$\frac{\Delta H_{r}^{o}}{RT} = \sum_{i=1}^{N}\left(v_{i,r}^{''} - v_{i,r}'\right)\frac{h_{i}^{o}}{RT} \tag{18}$$

Reactions Kinetics

The coal devolatilization reaction used for the present study which has been empirically discussed by *Kim et al.* [6], it was deduced from the thesis [16] and *Strezov et al.* [17] for the present study. In Table 5, eleven reactions reviewed by *Kim et al.* [6] described with their kinetics, while other seven additional reactions (proposed by *Wadhwani* [15]) with their kinetics are described in Table 6. A preliminary study showed the formed Fe_3O_4 coming from the fuel reactor is very low in molar concentration thus ignored in the present study.

Effect of pressure

Lindemann form is used in the present model, to represent the rate expression in pressure dependent reactions which makes a reaction dependent of both pressure and temperature. In Arrhenius form, the parameters for high pressure limit (k) and low pressure limit (k_{low}) are described as follows:

$$k = A_{r}T^{\beta}e^{-E/RT} \tag{19}$$

$$k_{low} = A_{low}T^{\beta_{low}}e^{-E_{low}/RT} \tag{20}$$

The net rate constant at any pressure is given by,

$$k_{net} = k\left(\frac{p_{r}}{1+p_{r}}\right)F \tag{21}$$

While, p_r is defined as,

$$p_{r} = \frac{k_{low}[M]}{k} \tag{22}$$

[M] is conc. of gas mixture, and function *F* is unity for Lindemann form.

Standard k-ε turbulence model:

The standard k-ε turbulence model was used for the present study

Eq. (23) is described for turbulent kinetic energy *k*

$$\frac{\partial(\rho k)}{\partial t} + \frac{\partial(\rho k u_{i})}{\partial x_{i}} = \frac{\partial}{\partial x_{i}}\left[\left(\mu + \frac{\mu_{t}}{\sigma_{k}}\right)\frac{\partial k}{\partial x_{j}}\right] + \tag{23}$$

$$G_{k} + G_{b} - \rho \in = -Y_{M} + S_{k}$$

And Eq. 24 is described for the rate of dissipation ε

Table 7: Computational and Simulation Parameters for the Present Study.

Parameters	Value
Operating Pressure	10 atm
Air Inlet Velocity	0.005 m/s
Fuel Flow rate for MC	1.18 kg/h
Fuel Flow rate for SBC	1.30kg/h
Air and Fuel inlet Temperature	320 K
Carrier CO_2 gas flow rate	10 LPM
Model Parameters	
Solver	Unsteady State, 2nd order implicit
Discretization Scheme	Second order Upwind
Pressure Velocity Coupling	SIMPLE
Convergence Criterion	10^{-5}

$$\frac{\partial(\rho\varepsilon)}{\partial t} + \frac{\partial(\rho\varepsilon u_i)}{\partial x_i} = \frac{\partial}{\partial x_i}\left[\left(\mu + \frac{\mu_t}{\sigma_k}\right)\frac{\partial(\rho\varepsilon)}{\sigma x_j}\right]+ \tag{24}$$

$$C_{1\varepsilon}\frac{\varepsilon}{k}\left(G_k + C_{3\varepsilon}G_b\right) - C_{2\varepsilon}\rho\frac{\varepsilon^2}{k} + S_\varepsilon$$

Where, G_k is calculated by Eq. 25, G_b is calculated by Eq. (26), Y_M is calculated by Eq. 27

$C_{1\varepsilon}$, $C_{2\varepsilon}$, $C_{3\varepsilon}$ are the constants ($C_{1\varepsilon}$ = 1.44, $C_{2\varepsilon}$ =1.92)

σ_k =1, σ_ε =1.3

$$G_k = -\rho\overline{u_t'u_J'}\frac{\partial u_j}{\partial x_i} \tag{25}$$

$$G_b = \beta g_i \frac{\mu_t}{pr_t}\frac{\partial T}{\partial x_i} \tag{26}$$

Where, $Pr_t = 0.85$

$$Y_M = 2\rho\varepsilon M_t^2 \tag{27}$$

$$M_t = \sqrt{k/a^2} \quad \text{and} \quad a = \sqrt{\gamma RT}$$

Modeling the Turbulent Viscosity

The turbulent viscosity μ_t is calculated from Eq. (28)

$$M_t = \rho C_\mu \frac{k^2}{s} \tag{28}$$

Where, C_μ is a constant = 0.09

SOLUTION TECHNIQUE

The boundary condition for air and coal inlets were defined as velocity and mass flow inlet; and for the fuel reactor, and the cyclone exhaust as pressure outlets with no-slip conditions was kept at the wall boundary. The grid independence test was carried out on mesh size range from 0.005-0.025 (m) at steps of 0.005 (m), from which mesh size for the present unsteady state simulations was obtained to be 0.01 (m) and a time step of 0.001s with 40 iteration/time step. The details of solution techniques used in this simulation discussed in Table 7.

RESULTS AND DISCUSSION

In Table 8, the mass weighted average rate of reactions discussed in Table 5 & 6 for MC are computed from the CFD model for the first and the second. It shows that for the first set, Reactions (1.1), (8), (10), and (10 & 11) are prevailing in the fuel reactor, interconnecting

145

Table 8: Mass weighted average rate of reactions for MC for the first and second (shown in parenthesis ()*) set

Reaction number	Mass weighted average Rate of Reaction in Fuel reactor (kmol/m³-s)	Mass weighted average Rate of Reaction in inter-connecting pipe (kmol/m³-s)	Mass weighted average Rate of Reaction in Air reactor (kmol/m³-s)	Mass weighted average Rate of Reaction in riser section (kmol/m³-s)
1.1	8.16×10^{-4} $(1.03 \times 10^{-2})*$	2.68×10^{-8} $(7.448 \times 10^{-5})*$	0 $(0)*$	0 $(0)*$
2	6.52×10^{-7} $(1.09 \times 10^{-8})*$	2.83×10^{-10} $(2.35 \times 10^{-9})*$	0 $(0)*$	0 $(0)*$
3	3.89×10^{-10} $(6.10 \times 10^{-8})*$	0 $(0)*$	0 $(0)*$	0 $(0)*$
4	2.51×10^{-11} $(6.95 \times 10^{-9})*$	1.61×10^{-15} $(0)*$	0 $(0)*$	0 $(0)*$
5	7.49×10^{-9} $(3.07 \times 10^{-8})*$	1.34×10^{-14} $(0)*$	0 $(0)*$	0 $(0)*$
6	0 $(1.83 \times 10^{-9})*$	9.79×10^{-10} $(1.56 \times 10^{-10})*$	5.76×10^{-11} $(2.92 \times 10^{-11})*$	1.49×10^{-12} $(3.89 \times 10^{-20})*$
7	0 $(2.31 \times 10^{-9})*$	3.31×10^{-11} $(1.47 \times 10^{-9})*$	8.36×10^{-12} $(2.78 \times 10^{-10})*$	4.82×10^{-12} $(1.32 \times 10^{-11})*$
8	2.47×10^{-6} $(3.09 \times 10^{-11})*$	1.08×10^{-6} $(8.46 \times 10^{-13})*$	0 $(2.11 \times 10^{-13})*$	0 $(8.94 \times 10^{-30})*$
9	4.24×10^{-14} $(1.52 \times 10^{-10})*$	0 $(0)*$	0 $(0)*$	0 $(0)*$
10	0 $(0)*$	0 $(0)*$	3.81×10^{-8} $(3.58 \times 10^{-5})*$	2.13×10^{-9} $(6.80 \times 10^{-6})*$
11	0 $(0)*$	0 $(0)*$	7.49×10^{-10} $(2.01 \times 10^{-11})*$	3.62×10^{-9} $(2.17 \times 10^{-11})*$
12	- $(3.22 \times 10^{-14})*$	- $(1.53 \times 10^{-14})*$	- $(8.66 \times 10^{-16})*$	- $(3.64 \times 10^{-36})*$
13	- $(4.29 \times 10^{-5})*$	- $(1.21 \times 10^{-4})*$	- $(-6.77 \times 10^{-7})*$	- $(-6.31 \times 10^{-7})*$
14	- $(5.40 \times 10^{-4})*$	- $(1.22 \times 10^{-4})*$	- $(5.06 \times 10^{-5})*$	- $(1.92 \times 10^{-5})*$
15	- $(0)*$	- $(0)*$	- $(3.24 \times 10^{-5})*$	- $(1.29 \times 10^{-9})*$
16	- $(0)*$	- $(0)*$	- $(4.87 \times 10^{-6})*$	- $(7.76 \times 10^{-8})*$
17	- $(7.21 \times 10^{-13})*$	- $(4.05 \times 10^{-13})*$	- $(6.91 \times 10^{-14})*$	- $(3.60 \times 10^{-15})*$
18	- $(0)*$	- $(0)*$	- $(2.63 \times 10^{-6})*$	- $(2.49 \times 10^{-29})*$

(a) Contour of Velocity

(b) Contour of Total temperature
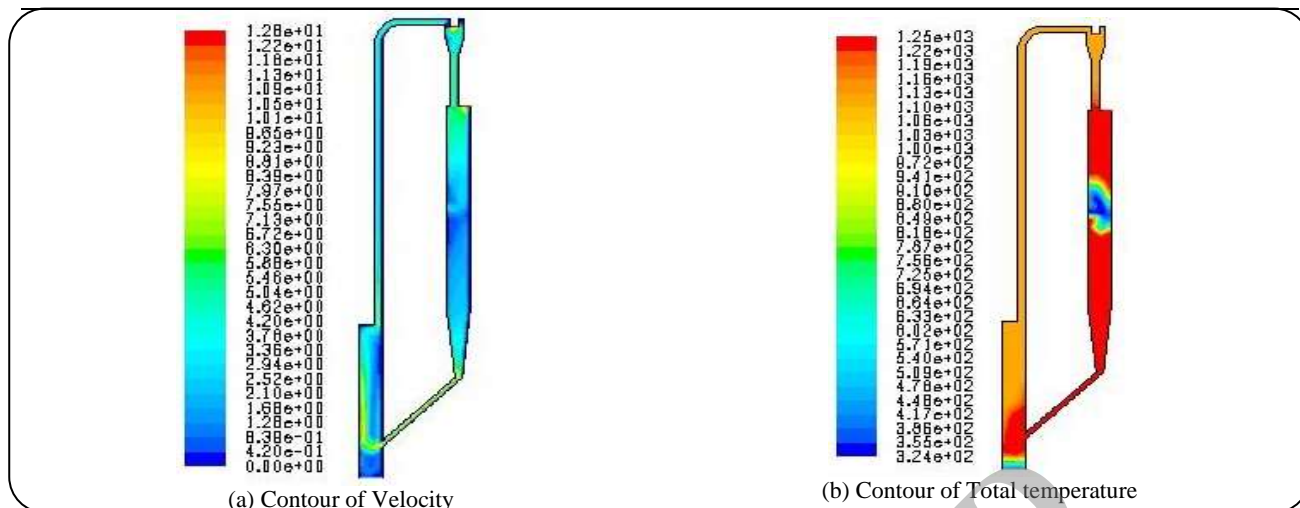
Fig. 3: Contours of Velocity and Total Temperature for MC for the second set.

(a) Contour of water

(b) Contour of oxygen

(c) Contour of Nitrogen

(d) Contour of Iron

(e) Contour of iron (III) oxide

(f) Contour of carbon

Fig. 4: Molar concentration contour for MC for the second set.

147

(g) Contour of carbon monoxide   (h) Contour of carbon dioxide   (i) Contour of MC
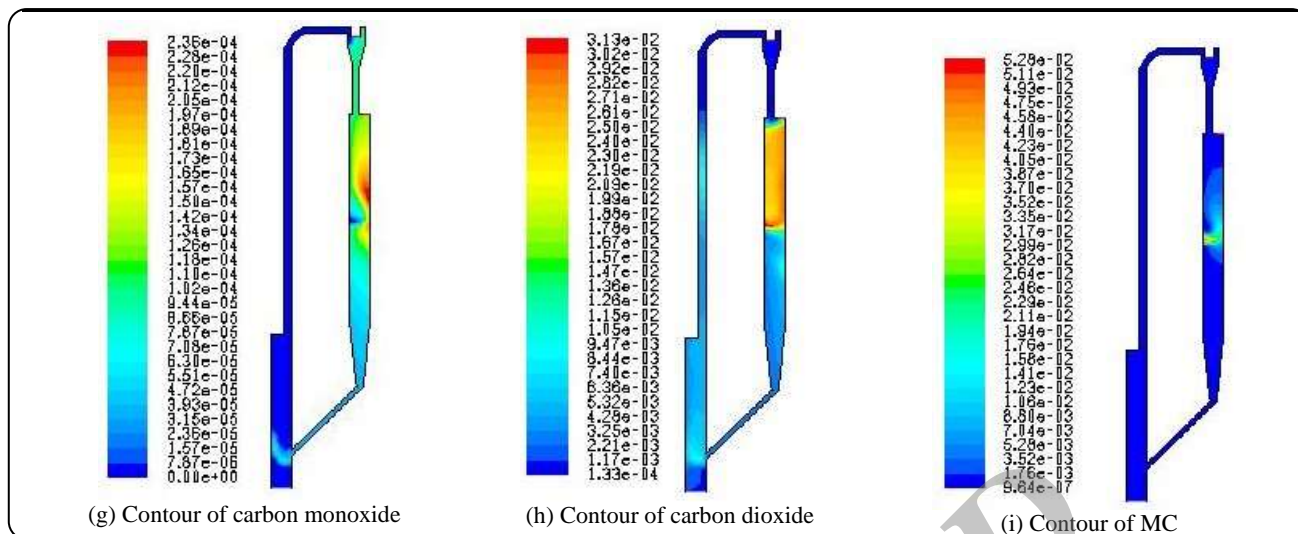
Fig. 4: Molar concentration contour for MC for the second set.

parts, the air reactor, and the riser section of the process respectively. While, in the second set of reactions, Reactions (1.1), (13 & 14), (10 & 15), and (14) which are altogether different except Reaction 1.1 are prevailing in the fuel reactor, interconnecting parts, the air reactor and the riser sections respectively.

In the second set, steam reforming and water-gas shift are the most dominating reactions taking place in the interconnecting part which join the two reactors where methane/carbon monoxide, and steam reacts due to confined channel for their flow. In the air reactor, the reaction no. 15 (burning of residual carbon deposited on the oxygen carrier) shows a relative dominance in comparison to reaction no. 10 (oxidation of iron to ferric oxide) as visible from the mass weighted average rate of reactions.

Fig. 3 shows the velocity and the temperature profiles for the process. The temperature profile (Fig. 3b) shows discontinuity in the fuel reactor which is due to the presence of fuel inlet marked as "A" in Fig.1. Fig.4 shows the molar concentration for some species when the second set of reactions are employed. The presence of very low quantity (almost absence) of nitrogen and oxygen (Fig. 4c and 4b) in the fuel reactor meets the principal objective of the chemical looping process which avoids the energy penalty during the separation of carbon dioxide and nitrogen in the fuel reactor exhaust. The presence of slight amount of carbon and carbon monoxide (Fig. 4f and 4g) in the air reactor due to seepage of left over carbon and carbon monoxide from the fuel reactor justifies the inclusion of reaction nos. 15 and 16. The mass average velocities for the fuel reactor exhaust for the first and the second set are 8.45 and 5.81 m/s respectively. From the molar concentration of MC (Fig. 4i) with time the conversion of fuel is computed.

Table 9, shows the comparison between the model predictions between the both sets of reactions and that of sub-pilot plant results. It is quite visible that the predictions for the second set are within an error band of ±12% while these are within -13% to +16% for the first set.

Similarly to MC, the mass weighted average rate of reactions obtained for SBC by both sets are discussed in Table 10. It is visible that the Reactions (1.2), (6 & 8), (10), and (10) are prevailing in the fuel reactor, interconnecting parts, the air reactor and the riser section of the process respectively in the first set. While, Reactions (1.2), (6 & 14), (10 & 18), and (13 & 14) are dominating in the second set. The carbon monoxide reduction of ferrous oxide (reaction no. 6) and steam reforming reaction (reaction no. 14) are the dominant reactions in the interconnecting part for SBC which are different from that of MC. This difference is possibly due to higher value of carbon percentage and calorific value in MC (Table 2).

148

Table 9: Verification of present CFD model for MC.

Parameter	Predicted Values for Set 1	Predicted Values for Set 2	Pilot plant values	Error in Set 1	Error in Set 2
Fuel (MC) Conversion (on dry ash free basis)	83.24%	87.07%	70-99%	15.91%	12.05%
Fuel Reactor Exhaust Mole Fraction on dry and nitrogen free basis					
CO_2	86.27%	90.19%	99.8%	13.56%	9.63%
CO	0.153%	0.146%	0.14%	-9.29%	-4.28%
CH_4	0.053%	0.058%	0.06%	11.66%	3.33%
Cyclone Exhaust Mole Fraction					
O_2	21.89%	21.02%	19.5%	-12.26%	-7.79%
CO_2	0.065%	0.079%	0.07%	7.14%	-11.39%
CH_4	0.0134%	0.0167%	0.015%	10.66%	-11.33%

Table 10: Mass weighted average rate of reactions for SBC for the first and the second (shown in parenthesis ()*) set

Reaction number	Mass weighted average Rate of Reaction in Fuel reactor (kmol/m³-s)	Mass weighted average Rate of Reaction in inter-connecting pipe (kmol/m³-s)	Mass weighted average Rate of Reaction in Air reactor (kmol/m³-s)	Mass weighted average Rate of Reaction in riser section (kmol/m³-s)
1.2	1.3×10^{-4} (3.48×10^{-3})*	2.8×10^{-7} (9.73×10^{-6})*	0 (0)*	0 (0)*
2	1.25×10^{-5} (4.94×10^{-5})*	4.94×10^{-7} (2.25×10^{-5})*	0 (0)*	0 (0)*
3	3.37×10^{-7} (7.04×10^{-9})*	0 (0)*	0 (0)*	0 (0)*
4	3.04×10^{-7} (1.91×10^{-9})*	2.58×10^{-7} (0)*	0 (0)*	0 (0)*
5	3.22×10^{-14} (1.65×10^{-8})*	4.54×10^{-14} (0)*	0 (0)*	0 (0)*
6	0 (9.17×10^{-5})*	5.38×10^{-3} (4.59×10^{-4})*	5.01×10^{-7} (3.26×10^{-7})*	1.87×10^{-9} (7.09×10^{-10})*
7	0 (2.98×10^{-11})*	2.00×10^{-10} (2.66×10^{-5})*	1.47×10^{-11} (1.79×10^{-9})*	3.13×10^{-14} (5.51×10^{-9})*
8	3.31×10^{-5} (3.77×10^{-4})*	1.43×10^{-3} (1.97×10^{-5})*	0 (7.84×10^{-9})*	0 (3.34×10^{-21})*
9	2.91×10^{-10} (8.34×10^{-12})*	0 (0)*	0 (0)*	0 (0)*
10	0 (0)*	0 (0)*	5.52×10^{-5} (1.08×10^{-4})*	5.34×10^{-7} (1.45×10^{-10})*
11	0 (0)*	0 (0)*	5.65×10^{-8} (1.50×10^{-9})*	5.91×10^{-9} (8.43×10^{-11})*
12	- (3.12×10^{-15})*	- (5.04×10^{-15})*	- (9.72×10^{-17})*	- (9.75×10^{-39})*
13	- (7.57×10^{-4})*	- (-1.09×10^{-5})*	- (-6.34×10^{-5})*	- (-1.41×10^{-6})*
14	- (2.71×10^{-4})*	- (1.07×10^{-4})*	- (9.36×10^{-5})*	- (2.56×10^{-6})*
15	- (0)*	- (0)*	- (8.76×10^{-5})*	- (2.04×10^{-30})*
16	- (0)*	- (0)*	- (6.89×10^{-5})*	- (1.22×10^{-15})*
17	- (2.58×10^{-9})*	- (5.03×10^{-9})*	- (6.46×10^{-11})*	- (1.04×10^{-9})*
18	- (0)*	- (0)*	- (3.6×10^{-4})*	- (1.04×10^{-9})*

Table 11: Verification of present CFD model for SBC.

Parameter	Predicted Values for set 1	Predicted Values for set 2	Pilot plant values	Error in set 1	Error in set 2
Fuel (SBC) Conversion (on dry ash free basis)	89.81%	95.39%	97-99%	9.28%	3.64%
Fuel Reactor Exhaust Mole Fraction on dry and nitrogen free basis					
CO_2	88.98%	92.34%	99.6%	10.66%	7.28%
CO	0.067%	0.091%	0.08%	16.25%	-13.75%
CH_4	0.219%	0.241%	0.25%	12.4%	3.6%
Cyclone Exhaust Mole Fraction					
O_2	16.82%	16.49%	18.5%	9.08%	10.86%
CO_2	0.12%	0.11%	0.1%	-20%	-10%
CH_4	0.023	0.017%	0.02%	-15%	15%

(a) Contour of Velocity   (b) Contour of Total Temperature
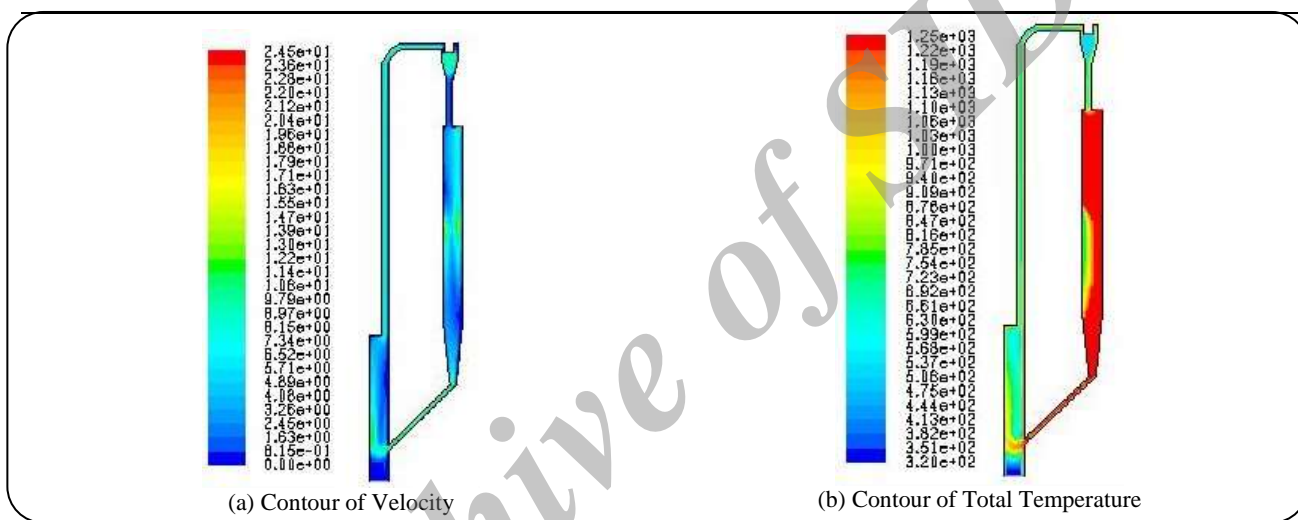
Fig. 5: Contours of Velocity and Total temperature for SBC for the second set.

For the second set of reactions, Fig. 5 shows the velocity and the temperature profiles of the system while Fig. 6, shows the molar concentration of some species such as nitrogen, oxygen, carbon and carbon dioxide (Fig. 6c, 6b, 6f, and 6g) are observed analogous to MC. Similar to MC, very low presence of nitrogen and oxygen is observed in the fuel reactor. Furthermore, similar presence of slight amount of carbon and carbon monoxide in the air reactor due to seepage from the fuel reactor strengthen the inclusion of Reactions 15 and 16. The mass average velocity for fuel reactor exhaust for the first and the second set of reactions are 3.02 and 7.79 m/s respectively. The conversion of fuel is computed from the change in molar concentration of SBC (Fig. 6i) with time.

Table 11, shows the comparison between the prediction of both sets of computational model and that of sub-pilot plant results. The predictions are within an error band of -14% to +15%, and -20% to +17% for the second and first set respectively. However, it is to be noted that the species having minor concentration (<0.3%) in the fuel reactor and cyclone exhaust exhibit higher simulation error in the second set, if ignore the effect of minor species then the error band reduces to +9% to +11%.

CONCLUSIONS

The salient findings of this study are as follows:

1. Results of present simplified 2D CFD model utilizing the first set of reactions are in acceptable agreement with the sub-pilot plant data. The simulated fuel conversions for the two fuels i.e. MC and SBC show an error of 15.91% and 9.28% respectively with the maximum fuel conversion.
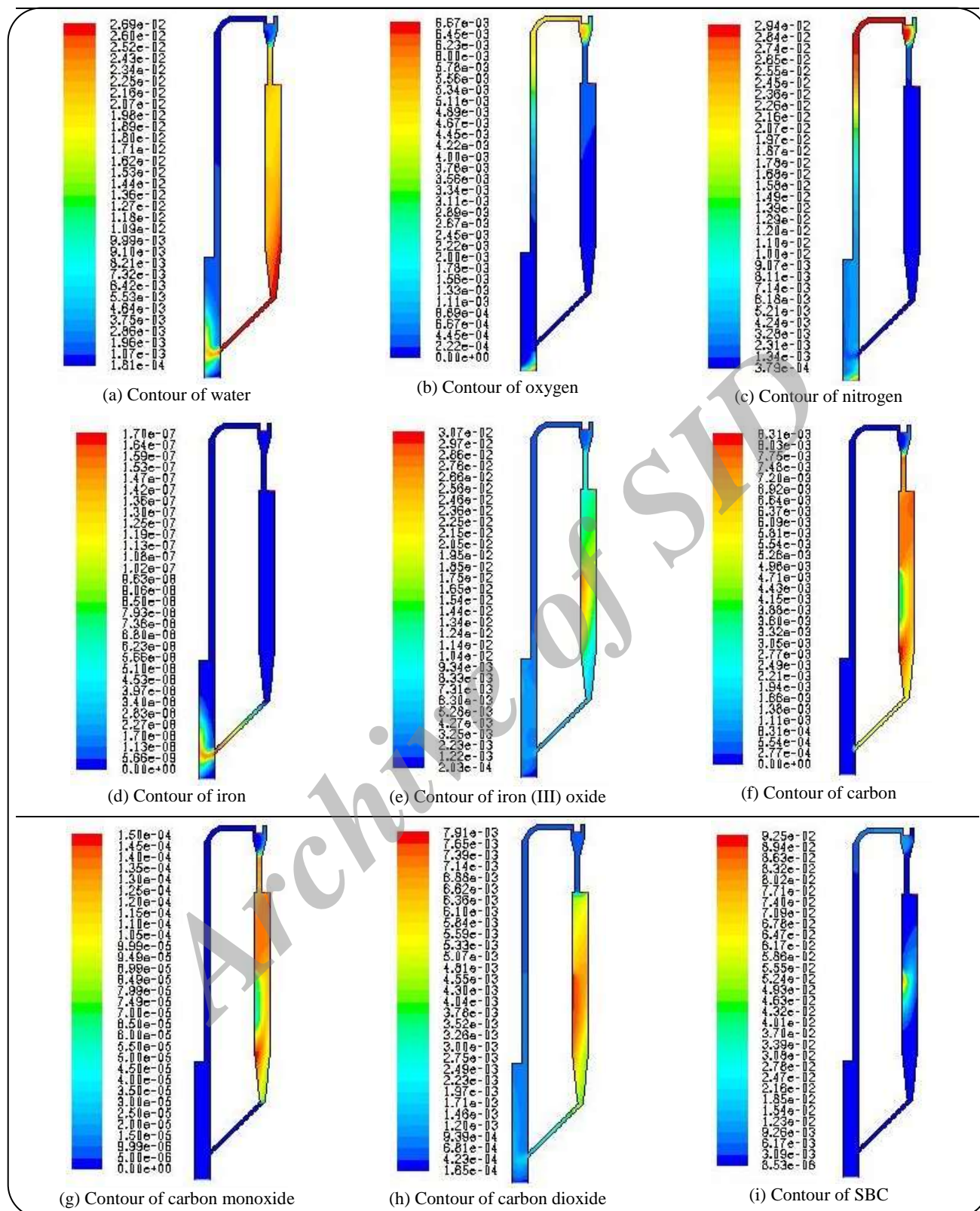
(a) Contour of water

(b) Contour of oxygen

(c) Contour of nitrogen

(d) Contour of iron

(e) Contour of iron (III) oxide

(f) Contour of carbon

(g) Contour of carbon monoxide

(h) Contour of carbon dioxide

(i) Contour of SBC

Fig. 6: Molar concentration contour for SBC for the second set.

151

2. Further utilizing the second set of reactions a better agreement achieved with the sub-pilot plant data. The simulated fuel conversions for MC and SBC show errors of 12.05% and 3.64% respectively with the maximum fuel conversion improving results by 4% and 6% with the first set of reaction.

3. Use of simplified 2D CFD model to simulate complex assembly is possible if the above error limit is under tolerance.

Nomenclature

A_r	Pre-exponential factor
β	Coefficient of thermal expansion
β_r	Temperature exponent
$C_{j,r}$	Molar concentration of species j in reaction r
$D_{i,m}$	Diffusion coefficient for the ith species in the mixture
ε	The rate of dissipation
E_R	Activation energy for the reaction
$\vec{F}$	External body forces and also contains user-defined terms
$\gamma_{j,r}$	Third-body efficiency of the jth species in the rth reaction
g_i	Gravitational vector in the ith direction
G_b	The generation of turbulence kinetic energy due to buoyancy
G_k	Generation of turbulence kinetic energy due to mean velocity gradients
h^0_i	Standard-state enthalpy (heat of formation) which are specified as properties for every species
$\vec{J}_t$	Diffusion flux of the ith species
$\vec{J}_j$	Diffusion flux of species j
K	Turbulent kinetic energy
$k_{b,r}$	Backward rate constant for reaction r
k_{eff}	Effective conductive $(=k+k_t)$
$k_{f,r}$	Forward rate constant for reaction r
k_t	Turbulent thermal conductivity
K_r	Equilibrium constant for the rth reaction
M	Molecular viscosity
μ_t	Turbulent viscosity
M_i	Symbol denoting species i
M_t	Turbulent Mach number
$M_{w,i}$	Molecular weight of ith species

$\eta'_{j,r}$	Rate exponent for reactant species j in reaction r
$\eta''_{j,r}$	Rate exponent for product species j in reaction r
N	Number of chemical species in the system
P	Static pressure
p_{atm}	Atmospheric pressure (101.325 kPa)
Pr_t	Turbulent Prandtl number for energy
$\rho\vec{g}$	Gravitational body force
R	Universal gas constant
R_i	Net rate of production of species i by chemical reaction
$\widehat{R}_{i,r}$	Arrhenius molar rate of creation/destruction of species i^{th} in reaction r
σ_ε	Turbulent Prandtl number for ε
σ_k	Turbulent Prandtl number for k
S_ε	User defined source term
S_h	The heat of chemical reaction and any other volumetric source by user defined function
S_i	Rate of creation by addition from dispersed phase plus any user defined sources
S^0_i	Standard-state entropy which are specified as properties for every species
S_k	User defined source term
S_m	Mass added to continuous phase from second phase or any user-defined sources
$\overline{\overline{\tau}}$	Stress tensor
Γ	The net effect of third bodies on the reaction rate
$v'_{i,r}$	Stoichiometric coefficient for reactant i in reaction r
$v''_{i,r}$	Stoichiometric coefficient for product i in reaction r
Y_j	The mass fraction of species j
Y_M	The contribution of the fluctuating dilation in compressible turbulence to the overall dissipation rate

REFERENCES

[1] BP Statistical Review of World Energy, June (2013).

[2] National Council for Science and the Environment, "Energy for a Sustainable and Secure Future: A Report of the Sixth National Conference on Science, Policy and the Environment", Edited by D. E. Blockstein and M. A. Shockley, Washington DC, (2006).

152

[3] Lyngfelt A., Oxygen Carriers for Chemical Looping Combustion - 4000 h of Operational Experience, *Oil Gas Sci. Technol.*, **66**: 161-172 (2011).

[4] Abad A., Mattisson T., Lyngfelt A., Rydén M., Chemical-Looping Combustion in a 300 W Continuously Operating Reactor System Using a Manganese-Based Oxygen Carrier, *Fuel*, **85**: 1174-1185 (2006).

[5] Berguerand N., Lyngfelt A., The Use of Petroleum Coke as Fuel in a 10 kW$_{th}$ Chemical-Looping Combustor, *Int. J. Greenh. Gas Contro*l, **2**(2): 169-179 (2008).

[6] Kim H. R., Wang D., Zeng L., Bayham S., Tong A., Chung E., Kathe M. V., Luo S., McGiveron O., Wang A., Sun Z., Chen D., Fan L.S., Coal Direct Chemical Looping Combustion Process: Design and Operation of a 25-kWth Sub-Pilot Unit, *Fuel*, **108**: 370-384 (2013).

[7] Deng Z., Xiao R., Jin B., Song Q., Huang H., Multiphase CFD Modeling for a Chemical Looping Combustion Process (Fuel Reactor), *Chem. Eng. Technol.,* **31**: 1754-1766 (2008).

[8] Emden H. K., Rickelt S., Stepanek F., Munjiza A., Development and Testing of an Interconnected Multiphase CFD-Model for Chemical Looping combustion, *Chem. Eng. Sci.*, **65**: 4732-4745 (2010).

[9] Xiao R., Song Q., Song M., Lu Z., Zhang S., Shen L., Pressurized Chemical-Looping Combustion of Coal with an Iron Ore-Based Oxygen Carrier, *Combust. Flame*, **157**: 1140-1153 (2010).

[10] Lyngfelt A., Leckner B., Mattisson T., A Fluidized Bed Combustion Process with Inherent CO$_2$ Separation; Application of Chemical Looping Combustion, *Chem. Eng. Sci.*, **56**: 3101-3113 (2001).

[11] Luo M., Wang S., Wang L., Lv M., Qian L., Fu H., Experimental Investigation of co-Combustion of Coal and Biomass Using Chemical Looping Technology, *Fuel process. Technol.*, **110**: 258-267 (2013).

[12] Jin H., Ishida M., A New Type of Coal Gas Fueled Chemical Looping Combustion, *Fuel*, **83**: 2411-2417 (2004).

[13] Labiano F.G., Adanez J., de Diego L.F., Gayán P., Abad A., Effect of Pressure on the Behavior of Copper-, Iron-, and Nickel- Based Oxygen Carriers for Chemical Looping Combustion, *Energ. Fuel*, **20**: 26-33 (2006).

[14] Tian H., Chaudhari K., Simonyi T., Poston J., Liu T., Sanders T., Veser G., Siriwardane R., Chemical Looping Combustion of Coal Derived Synthesis Gas Over Copper Oxide Oxygen Carriers, *Energ. Fuel*, **22**: 3744-3755 (2008).

[15] Wadhwani R., "CFD Study of a Coal Direct Chemical Looping Pilot Plant", Dissertation, Indian Institute of Technology Roorkee, June (2014).

[16] Govind, "Modeling & Simulation of Gasification of Indian Coal", Dissertation, Indian Institute of Technology Roorkee, June (2012).

[17] Strezov V., Lucas J. A., Strezov L., Quantifying the Heats of Coal Devolatilization, *Metall. Mat. Tran. B,* **31B**: 1125-1131 (2000).

153